Thermal Analysis of MVDC Power Corridor

M. McCandless, C. Cooke,
J. Chalfant, C. Chryssostomidis
Sea Grant Design Laboratory
Massachusetts Institute of Technology
Cambridge, Massachusetts 02139
meganmcc@mit.edu

A. Colavitto, A. Vicenzutti,
A. Contin, G. Sulligoi
Dept. of Engineering and Architecture
University of Trieste
Trieste, Italy
andrea.colavitto@phd.units.it

***Abstract*— MIT Sea Grant has introduced the concept of the modular Integrated Power and Energy Corridor, which combines the majority of power for the ship into a small space making the thermal conditions of the corridor of great interest. This work quantified the effect of the current harmonics on the Joule losses and the resulting temperature field in a three-dimensional model of a Medium Voltage Direct Current (MVDC) multi-cable conduit, simulating two different geometries (four 1000A cables and sixteen 250A cables) at three different air flow conditions each, under representative current loading. It was discovered that the 1000A cases exceeded the acceptable temperature limits, while all the 250A cases were cool enough for use. To reduce the power corridor complexity, this study recommends the use of the 250A, no-air-flow case.**

Keywords—MVDC, Power Distribution, Skin Effect, Air Cooling, Modular Integrated Power and Energy Corridor

I. INTRODUCTION

Today's electrical power distribution systems can be designed in a completely different manner than in the past, due to the huge improvements in power electronic technologies. Furthermore, the shipboard demand for electric power has become greater over the years, and will probably continue to grow in the future. Therefore, new power system architectures can be exploited to increase the performance of the ship's Integrated Power System (IPS) [1]. The most innovative one is the Medium Voltage Direct Current (MVDC) distribution [2], providing several advantages:

- Pervasive static power converters that enable bidirectional power flow, active current limiting, and galvanic isolation [3];
- Power system compactness, and easier integration of additional functionalities [4];
- Easier integration of mission systems and hotel loads such as variable speed motors and LED lighting that require DC power [5] [6].

On the other hand, MVDC power distribution presents some issues that need to be solved. DC fault protection provides a challenge due to the lack of a natural zero-crossing of the current waveform, causing DC circuit breakers at the required voltage and current to be large, heavy and expensive; however, ongoing research is developing new solutions [7].

This material is based upon research supported by the U.S. Office of Naval Research (ONR) under award number ONR N00014-16-1-2945 Incorporating Distributed Systems in Early-Stage Set-Based Design of Navy Ships; ONR N00014-16-1-2956 Electric Ship Research and Development Consortium; by the National Oceanic and Atmospheric Administration (NOAA) under Grant Number NA14OAR4170077 - MIT Sea Grant College Program; and by the Massachusetts Institute of Technology Undergraduate Research Opportunities Program. This paper was approved for public release by ONR under DCN #43-5122-19.

Another possible issue is related to the presence of a large number of power-electronic devices connected to the same bus which may result in an increase in the harmonic pollution of the onboard distribution system. Consequently, additional power losses may be induced in the cables due to skin effects [8], resulting in higher cable temperatures. This may negatively affect the life expectancy of the insulation systems, leading to an increased number of failures. Thus, at present there is an interest in investigating the correlation between the cable electrical losses and the harmonic pollution, both in AC [9] and in DC [10] cables.

Recently, MIT Sea Grant has been focusing on developing new concepts for power distribution on an all-electric surface ship, introducing and championing the concepts of the Power Corridor and Reserved Space [11]. The Power Corridor combines the distribution, conversion, isolation, and storage of main bus power throughout the ship into one entity, which creates advantages in cost, survivability, and arrangement. Because the modular Integrated Power and Energy Corridor (IPEC) combines the majority of the power for the all-electric ship into a small space, and it is based on static power conversion technology, the thermal conditions of the corridor are of great interest.

Therefore, the objective of this work is to evaluate the power losses in multiple MVDC cable pairs supplying a set of power converters through taps, and then quantify the temperature field in a three-dimensional model of a cable conduit. The evaluation of the power losses is achieved by simulating the cables and taps under full load conditions, in the presence of harmonic pollution; the results of the electrical simulations are then used to perform a thermal analysis. The themal analysis is used to verify that the cable insulation does not exceed its allowable temperature; to define the air temperature in the cable conduit that allows safe operating conditions; and to evaluate the temperature of the cable conduit top and the effect on the equipment located above the conduit.

The paper is organized as follows: Section II outlines the case study used in this paper, while Section III describes how the models have been implemented for the study. Section IV and V present the results of the electrical and thermal analyses. Finally, Section VI presents the paper conclusions.

II. CASE STUDY CONFIGURATION

In order to evaluate the cooling required by the sample IPEC [11] shown in Fig. 1, two aspects must be considered: modeling the thermal effect of the current's harmonic content due to power electronics; and analyzing the temperature trend along the IPEC. Therefore, different configurations of cables and different air flow conditions within the cable conduit have been considered, to determine

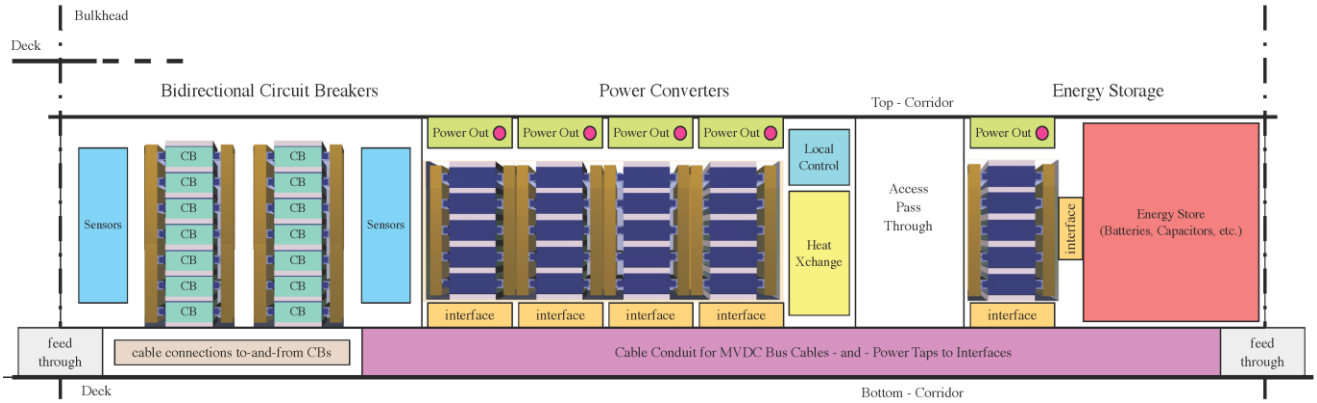

Fig. 1. Side view of sample power corridor [11]. In pink the Cable Conduit for MVDC Bus Cables and Power Taps to Interfaces.

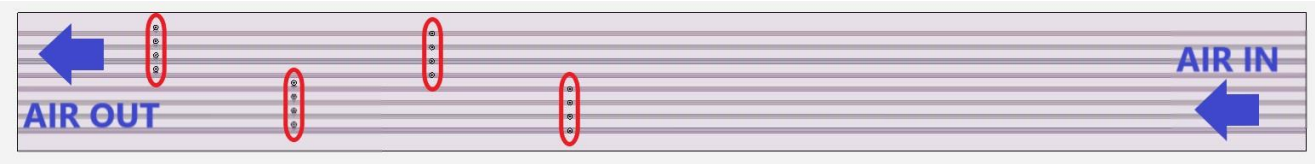

Fig. 2. Top view of the Cable Conduit. Tap connections circled in red.

TABLE I. GEOMETRY SPECIFICATIONS FOR THE CABLES

	Cable Ampacity [A]	Conductor Diameter [mm]	Outer Diameter [mm]
Case A	1000	18.4	38.4
Case B	250	9.2	29.2
Tap	125	6.5	26.5

which conditions allow for the safer operation of the Power Corridor in an all-electric ship.

A. *Cable Conduit*

The study is focused specifically on the cable conduit, represented by the pink box at the bottom in Fig. 1. This conduit contains the main MVDC power cables and the taps to the interfaces, which in turn supply the power converters. Due to the bidirectional nature of the power converters, power can either enter or depart the main bus through these taps. The goal of this study is to understand temperature trends within the cable conduit under different component arrangements.

The section of the sample cable conduit modeled herein is 280 inches (7.11 m) in length, 30 inches (0.76 m) wide, and 15 inches (0.38 m) tall. The conduit is assumed to be an enclosed box with solid metal sides, bottom, and top. The ends of the conduit are open, allowing either forced or natural convection. A top view of the cable conduit is shown in Fig. 2. The schematic depicts *Case B*, as specified in Section II.C; however, the taps in all designs are located the same distance from the end of the cable conduit.

B. *Taps*

Four power converters were modeled in the case study, each supplied via from the main bus cables located in the cable conduit, via tee junction connections. Each converter requires 1 MW of power, which is supplied through two pairs of taps, positioned as shown in Fig. 2:

- Tap 1 and 2: 30 in. (0.76 m) from left end;
- Tap 3 and 4: 60 in. (1.52 m) from left end;
- Tap 5 and 6: 90 in. (2.28 m) from left end;
- Tap 7 and 8: 120 in. (3.04 m) from left end.

For redundancy purposes, only one of each pair of taps (e.g. 1 or 2, 3 or 4, and so on) is operating at any time, resulting in maximum four simultaneous taps. A tap pair consists of one tap to the positive cable and one tap to the negative cable in a cable pair. Tap pair numbers are marked on the cables in Fig. 3 and 4.

C. *Main Bus Power Cables*

The conduit is designed to carry 24 MW, with a 20% installed margin already included, at +/- 6 kVdc. The cables are arranged in pairs, alternating polarity both horizontally and vertically to preserve symmetry. Tap cables leading to and from power converters are sized at 125 A. Two main bus cable configurations that differ in the number and type of cables used were considered in this paper:

- *Case A*: the main bus cables have an ampacity of 1000 A. There are two pairs of cables, each supplying four taps as shown in Fig. 3. In this case each cable has four taps, one at each location for the taps, as represented by the numbers adjacent to each cable.
- *Case B*: the main bus cables have an ampacity of 250 A. There are eight pairs of cables, each feeding a single tap, as depicted in Fig. 4. In this case, its number on each cable determines the single tap connected to that cable.

All the cables consist of a copper conductor and a cross-linked polyethylene (XLPE) insulation layer of 10 mm thickness (inner layer detail is not shown in the figures). The geometry specifications for each case are reported in Table I.

Note that the main bus cable sizes were selected to maintain an equal current density (i.e. 3.76 A/mm^2) in both cases. Therefore, the power losses in each configuration should be constant, with the exception of skin effects. The latter effect is expected to be significant, thus it is evaluated in the following. Despite fixing the same current density, temperature differences among the cables are still expected due to the differences in the cable surface area to cross-sectional area ratio.

TABLE II. HARMONIC CONTENT USED IN THE SIMULATIONS

Frequency [kHz]	0.5	2	2.5	4	10	10, π/4 phase shift
Amplitude %	4	2	2	1.5	1.5	1

TABLE III. ANSYS 3D MODEL BOUNDARY CONDITIONS

	No air flow	**Ambient air flow**	**Chilled air flow**
Air Inlet velocity [m/s]	0	1	1
Air Inlet Temperature [°C]	33	33	12
Air Outlet Gauge Pressure [Pa]	0	0	0
Air Outlet Temperature [°C]	33	Not required	Not required
Cable Temperature at Conduit Ends [°C]	65	65	65
Power Corridor Wall Conditions	Convection, Film coefficient: 4 W/m^{2}K, Ambient temp: 33°C		

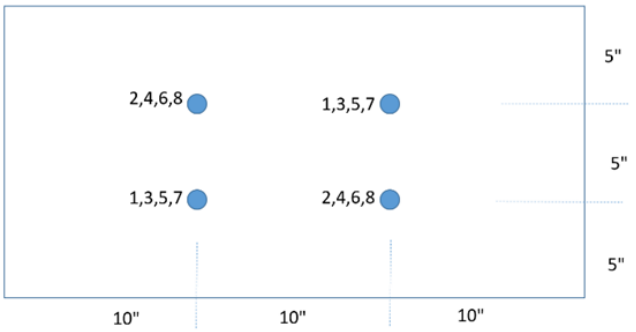

Fig. 3. Case A - four 1000 A cables (two pairs), frontal view.

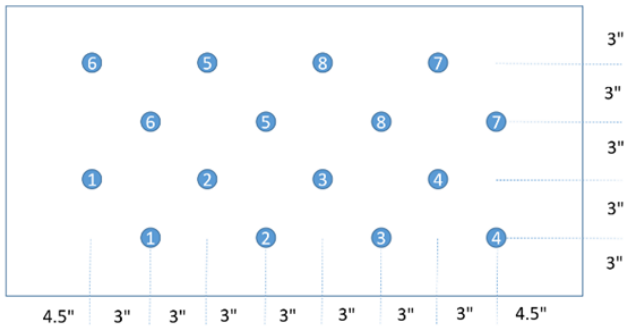

Fig. 4. Case B - sixteen 250 A cables (eight pairs), frontal view.

D. Harmonic Content

To simulate the effect of the power electronics operation, harmonic content was added to the steady state DC current as shown in Table II. The amplitude is represented as a percentage of the total DC component; one frequency also contains a phase shift.

III. MODEL IMPLEMENTATION

In this section, the electrical and thermal studies that were performed are briefly described, to specify how the results were reached using dedicated software tools.

First, the effect of the current harmonic content on the cables' power losses was evaluated for each case considered. COMSOL Multiphysics 5.2 (finite element software) was used to develop 2-D models of the cables in cross section and a complete 3-D model of the junction. The latter allowed the analysis of tee junction behavior, whose structure is more complex than the cable.

The Table I cases were applied to define the amount of power that is lost as heat along the cables and junctions. The finite element software allowed the evaluation of the increase in losses due to the skin effect without relying on empirical equations. Then, by using the power loss data calculated from the electrical analysis, it was possible to determine the temperature field in the cable conduit using ANSYS AIM Fluid-Solid Heat Transfer, a CFD solver. The two cable configurations that were simulated are shown in Fig. 3 (two 1000 A cable pairs) and in Fig. 4 (eight 250 A cable pairs). For each geometry, three thermal simulations were run:

- no air flow;
- ambient-temperature air flow;
- chilled air flow.

The boundary conditions used for the thermal simulation are reported in Table III. The air inlet is at the opposite side of the taps, as shown in Fig. 2. In the no-air-flow cases, an additional boundary condition was required to fully define the model, so the outlet temperature was set to 33°C, which is the same as the ambient temperature.

IV. ELECTRICAL SIMULATIONS

The simulations were conducted assuming maximum power flow through the conduit, as well as maximum power demand from each converter. Thus, the power flowing in the corridor at its input (left side of Fig. 2) is 24 MW at +/- 6kV. At each of the four operational power taps, 1 MW is diverted to the power converters installed on top of the conduit, yielding a load current of 83.333 A in each tap cable. The remaining 20 MW exits the conduit at the far end of the conduit, on the right side in Fig. 2.

At first, a three-dimensional simplified model of the tee junction was analyzed, to evaluate the skin effect in its geometry. The results are shown in Fig. 5, 6, and 7. The first figure shows the current density on the surface of the tee connector and related cables, for the first tap of *Case A*. The simulation was performed with a single fixed frequency current (i.e. 10 kHz), to evaluate the worst case. The deep red sections present a higher current density at the surface in respect to the dark blue ones. In Fig. 6 the same model is shown, this time highlighting the current density in a slice of the tee junction, as well as the magnitude and direction of the current flow (red arrows). Finally, Fig. 7 depicts the current density in the rectangular section of the connector. It is noticeable that the current density at a given frequency in the junction is appreciably lower than the density in both the main and tap cables. This is mainly due to two factors: the junction cross section is higher than the cables one (due to mechanical reasons); the rectangular shape of the connector limits the skin effect.

As can be seen from Fig. 5 and 6, the current in the connector presents very little skin effect and negligible localized density increases. Therefore, the losses due to the current harmonic content in the tap junctions was considered to be negligible. Moreover, the losses of the tee connector were neglected due to the low current density in the junction in respect to the cables. Consequently, a computational time saving is achieved when performing the thermal analyses, as discussed in Section V.

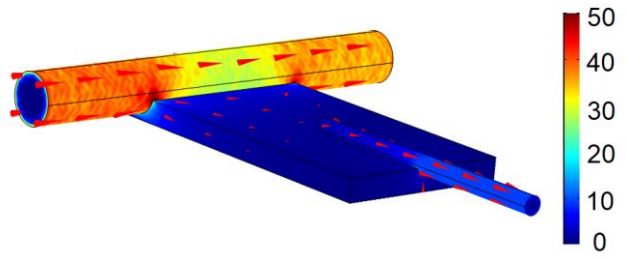

Fig. 5. Current density (A/mm^2) in a tee junction at 10 kHz - side view.

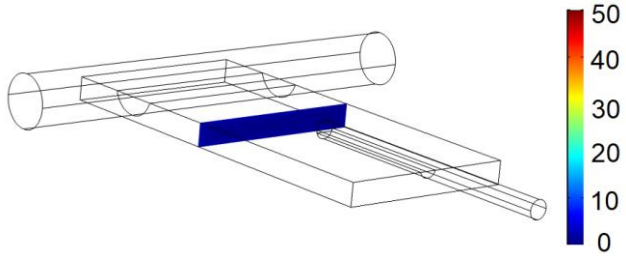

Fig. 6. Current density (A/mm^2) in a slice of the tee junction at 10 - side view.

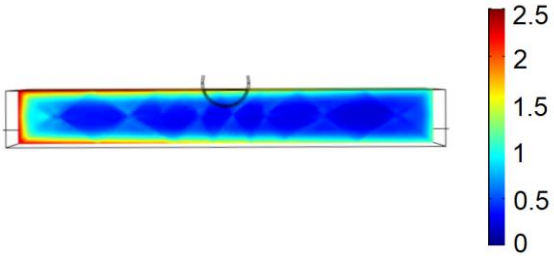

Fig. 7. Current density (A/mm^2) in a slice of the tee junction at 10 kHz – magnified front view.

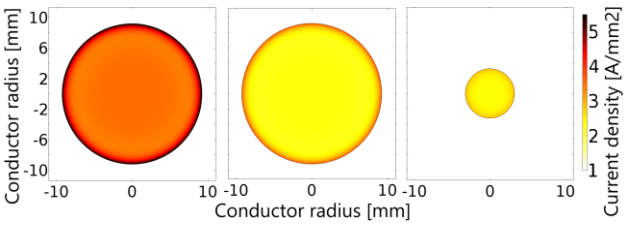

Fig. 8. *Case A* current density in cables cross section: prior to first tap (left), after fourth taps (center), tap cable (right)

TABLE IV. RESULTING POWER LOSSES IN THE CABLES

Case	Cable section	Power losses [W/m]
A	Prior to first tap	78.10256144
	Between first and second tap	65.64823993
	Between second and third tap	54.23031342
	Between third and fourth tap	43.9138765
	After fourth tap	34.72861953
B	Prior to tap	17.52710963
	After tap	7.789829618
Both	Tap cable	3.768483094

As a second step, the conductors' cross sections were simulated by means of 2-D models, to obtain their power losses. In this case, a time dependent simulation (200 ms length) was run, with the purpose of calculating the power losses' RMS value. To highlight the skin effect in the DC cables, in Fig. 9 a snapshot of the *Case A* current densities at 100 ms in three different cable sections is given. The shown cable sections are: prior to first tap (left); after fourth tap (center); tap cable (right). The current density scale range is the same for all sections. The losses resulting from the analyses for the two configurations are depicted in Table IV.

In *Case A*, since more than one tap is connected to the same cable, different cable sections were considered. Concerning the tap cables, they present the same power losses in both cases (since the current flowing in them the same). Clearly, the cables' losses reduce after each tap, due to the reduction of the flowing current (diverted into the tap cables).

V. THERMAL ANALYSIS

After having evaluated the power losses in each cable section, it is possible to analyze the thermal behavior of the cable conduit. The main modeling assumptions have been mentioned in Section II. However, an additional simplification was assumed after obtaining the electrical simulations results. In particular, the junctions proved to have a negligible contribution to the overall power losses. Thus, it was interesting to evaluate if their presence was significant or not concerning the thermal behavior of the system. To this aim, a detailed model of a single tap was built and simulated, showing a negligible difference in the results in respect to the simplified one. Therefore, the junctions were not modeled in the thermal analysis, thus reducing the simulations' complexity.

To evaluate the thermal behavior of the cable conduit, three sets of thermal data are of paramount importance: the internal cable temperature field; the air temperature field; and the cable conduit top-wall temperature field.

To condense the results, the maximum temperatures found for each of these locations is depicted in Table V. However, since in some cases the maximum temperature is not the most relevant value, a second temperature with an asterisk (*) before it is included, to indicate a more relevant value. This issue happens when a boundary condition directly causes the maximum temperature. In one case, a carat (^) indicates the approximate temperature of the cable near the tap, because the maximum temperature of the cable was caused by the boundary condition.

TABLE V. MAXIMUM TEMPERATURE VALUE FOR THE IPEC IN THE SIMULATED CASES

		No air flow [°C]	Ambient-temperature air flow [°C]	Chilled air flow [°C]
Case A - 1000A	*Cable*	175.68	150.84	127.06
	Air	149.85	127.01	102.89
	Wall	72.369 *57	58.835 *42	56.153 *29
Case B - 250A	*Cable*	98.154	72.213	65.00 ^50
	Air	90.741	65.873	60.008
	Wall	62.074 *54	53.377 *36	53.508 *26

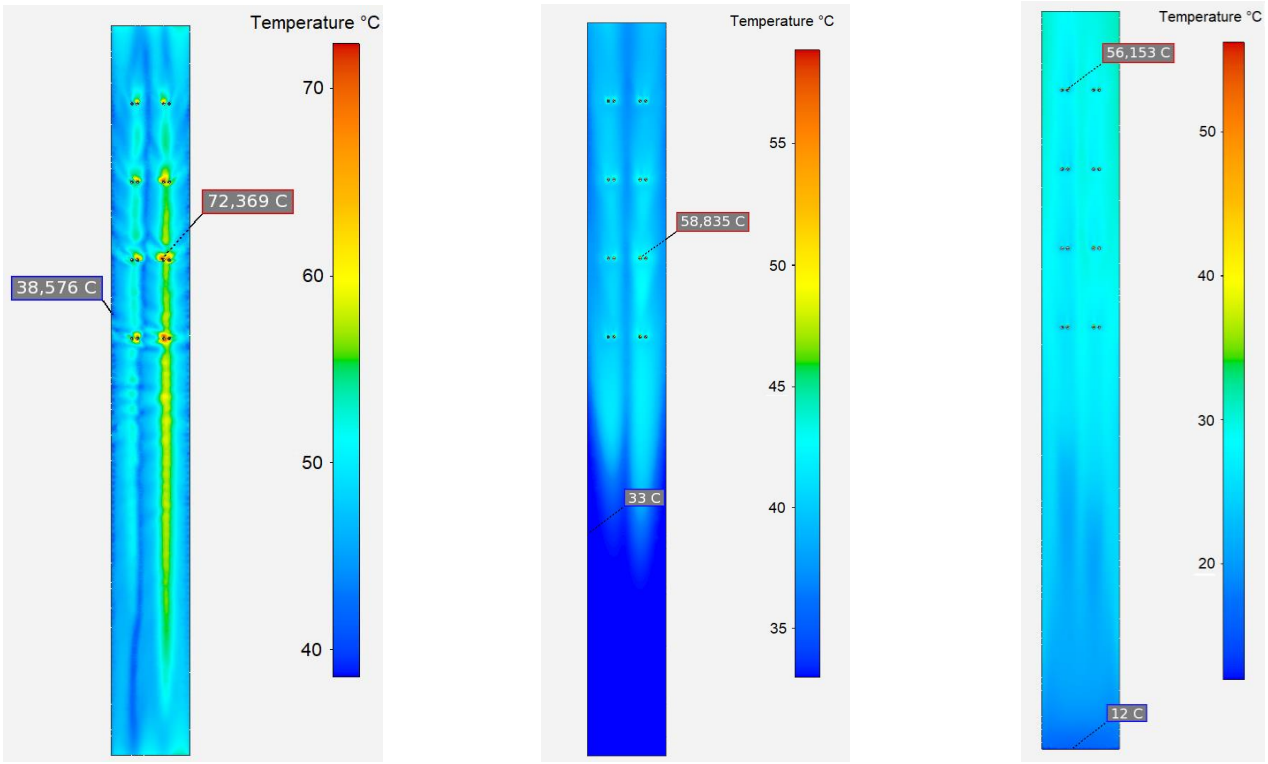

Fig. 9. Top view of *Case A* cable conduit for three air flow configurations: no air flow (left), ambient-temperature air flow (center) and chilled air flow (right). Air inlet at the bottom, outlet at the top

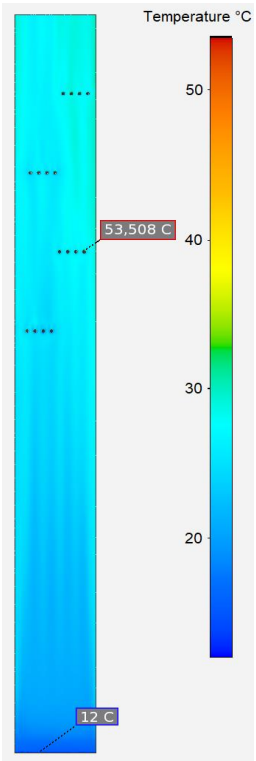

Fig. 10. Top view of *Case B*, chilled air flow. Air inlet at the bottom, outlet at the top

As can be seen in Table V, *Case A* shows much higher temperatures for all locations and air flow conditions. This is caused by the higher power traveling through each cable. Additionally, there is less total cable surface area in *Case A* than in *Case B*. The smaller the surface area, the less heat transfer can occur through convection (the primary form of heat transfer in these designs), and the higher the resultant temperature. Finally, it is relevant to notice that the temperatures for *Case A*, in all the performed simulations, may be so high as to impair the cable life expectancy.

A. Wall Temperatures

Fig. 9 shows top views of the cable conduit in *Case A*, for each possible air flow configuration. Note that in the figures, the color scale is determined by the maximum and minimum temperature in each simulation and is not set to a fixed value. This improves visualization of the change in temperature within each figure at the price of losing the possibility of directly comparing the figures.

In the no-flow case (Fig. 9, left) the maximum top wall temperature is 72.4°C. Since this maximum is a localized temperature spike, adjacent to a tap cable that penetrates the top surface of the conduit, it is not representative of the temperature of the overall top wall. In fact, most of the top wall is at a lower temperature, around 57°C, which is the one depicted in Table V with an asterisk.

In the ambient-temperature air flow case (Fig. 9, center) the maximum top wall temperature is 58.8°C, whereas most of the wall is at a lower temperature (circa 42°C).

In the chilled-air case (Fig. 9, right) the maximum wall temperature is 56.2°C, whereas most of the wall is at 29°C.

For *Case B*, in Fig. 10 the top wall temperature results are depicted for the chilled air flow condition. The figure can be directly compared with the right-hand image in Fig. 9. In all simulations, the temperatures in *Case B* are lower than those in *Case A*.

B. Bulk Air Temperatures

As expected, the no-air-flow condition produced the highest temperatures and chilled air flow produced the lowest. For most simulations, the bulk air is warmest at the outlet of the cable conduit and coolest at the inlet. In one case, *Case A* with no air flow, the highest air temperature is

found directly above the cables due to natural convection from the heat of the cables.

For *Case B*, a similar pattern emerged, with the chilled air flow having the lowest temperatures and the no-air-flow simulation having the highest temperatures. Further, all parts of *Case B* showed cooler temperatures than their respective *Case A* counterparts. Regarding inlet/outlet temperatures, *Case B* showed the same distribution of warm and cooler air as *Case A*: warmest at the outlet and coldest at the inlet.

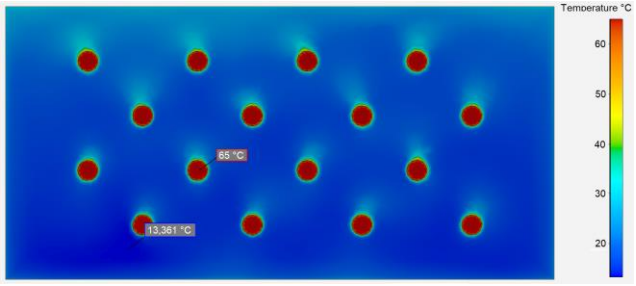

Fig. 11. Temperature distribution at *Case B* outlet, chilled air flow.

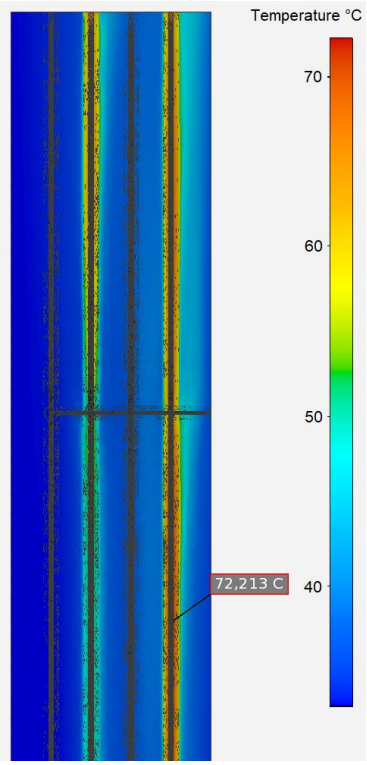

Fig. 12. Close up side cross section of the cable conduit in *Case B*, first tap, ambient temperature air flow. Top of the conduit on the right, bottom on the left, air inlet at the bottom, air outlet at the top.

Fig. 11 shows the temperature distribution at the outlet of *Case B* with chilled air flow. The maximum temperature in the cable in this simulation (65°C, occurring at the boundary) is caused by the boundary condition. Bulk air temperature increases in the vertical direction, even with chilled air flow. This effect is more apparent in the simulation with no air flow due to natural convection.

The taps' presence makes the surrounding air a little warmer, at the same time slowing the air flow because of their obstruction. In the no-flow cases, the taps create a pocket of hot air surrounding them, due to the natural convection effect.

C. Cable Temperatures

Fig. 12 displays a close-up of a cable conduit cross section in *Case B* with ambient-temperature air flow. The cross-sectional plane passes longitudinally through two cables, showing the insulation (the outer cable section ranging from light green to red) and the conductor within the cable (the darker middle section), as well as the distribution of temperature within them. The insulation is warmest at the boundary between the insulation and conductor, as expected, and cools as it nears the air where forced or natural convection occurs, depending on the test case.

The maximum temperature in the Fig. 12 case is 72.2 °C, located inside the cable. It is relevant to notice the difference between the second cable from the left and the fourth. The former is the one that is supplying the tap shown in the figure. Thus, it is possible to appreciate the difference in temperature before and after the tap, caused by the change in current level in the cable. In fact, part of the cable current that enters from the top is diverted into the tap, lowering the current amount that flows in the bottom cable section. In contrast, the fourth cable from the left is not connected to the tap shown in Fig. 12, thus showing a constant current flow and a near constant temperature. Finally, as expected, the heat is conducted along the cable conductor more readily than through the insulation into the surrounding air.

VI. Conclusions

In this paper, physics-based simulations of multiple cables located in a cable conduit have been performed in a configuration representative of the one required for the modular IPEC. The simulated cases evaluated herein included harmonic pollution data. The latter is representative of operational conditions for MVDC main bus cables in a power distribution system using significant amounts of power electronics. Through these simulations, it was possible to assess the increase in the losses caused by the harmonic pollution in the DC currents, as well as to evaluate the thermal behavior of some significant system configurations. The results show that configurations exist for which active thermal management is not required to maintain acceptable temperatures in the cables, insulation, surrounding air space, and conduit walls. It was also found that the design of the cable configuration for the system must include thermal considerations. This is demonstrated by the existence of configurations in which the temperatures are so high as to possibly impair the system life expectancy.

In particular, *Case A* (using two pairs of 1000 A cables) is very hot even with cooled air flow, making it a non-feasible configuration for the power corridor. Instead, *Case B* (using sixteen pairs of 250 A cables) has very reasonable temperatures under both ambient temperature air flow and no air flow, making the additional chilled air cooling not necessary.

Based on the above results, the best design for the cable conduit is 250 A cables with no air flow. Air flow provides an added complexity to the design of the IPEC that should be avoided if it can. The temperature of the cables is low enough that the insulation does not exceed its allowable temperature. While the maximum air temperature is quite warm, the average air temperature should be cool enough to provide workable conditions. Additionally, the top of the cable conduit is at a temperature sufficiently low to make it possible to keep the power electronics modules placed above it at reasonable temperatures, if some cooling is provided within them.

Finally, it should be noted that in this paper the effect of support structures, needed to hold the cables in position, on the heat dissipation was neglected. Further simulations should be done in more detail to shed more light on the issue.

The Cable Conduit is the backbone of the IPEC, and these preliminary simulations show that feasible designs exist, with no forced air flow, which can be easily implemented in the IPEC.

REFERENCES

[1] A. Vicenzutti, D. Bosich, G. Giadrossi, and G. Sulligoi, "The Role of Voltage Controls in Modern All-Electric Ships: Toward the all electric ship.," IEEE Electrification Mag., vol. 3, no. 2, pp. 49–65, Jun. 2015.

[2] N. Zohrabi, J. Shi, and S. Abdelwahed, "An overview of design specifications and requirements for the MVDC shipboard power system," Int. J. Electr. Power Energy Syst., vol. 104, pp. 680–693, Jan. 2019.

[3] D. Bosich, R. A. Mastromauro, and G. Sulligoi, "AC-DC interface converters for MW-scale MVDC distribution systems: A survey," in 2017 IEEE Electric Ship Technologies Symposium (ESTS), 2017, pp. 44–49.

[4] I. Chung et al., "Integration of a bi-directional dc-dc converter model into a large-scale system simulation of a shipboard MVDC power system," 2009 IEEE Electric Ship Technologies Symposium, Baltimore, MD, 2009, pp. 318-325.

[5] A. L. Gattozzi et al., "Power system and energy storage models for laser integration on naval platforms," in 2015 IEEE Electric Ship Technologies Symposium (ESTS), 2015, pp. 173–180.

[6] S. Hundertmark and O. Liebfried, "Power Supply Options for a Naval Railgun," ArXiv170905901 Phys., Sep. 2017.

[7] R. M. Cuzner and V. Singh, "Future Shipboard MVdc System Protection Requirements and Solid-State Protective Device Topological Tradeoffs," in IEEE Journal of Emerging and Selected Topics in Power Electronics, vol. 5, no. 1, pp. 244-259, March 2017.

[8] N. Idir, Y. Weens, and J. Franchaud, "Skin effect and dielectric loss models of power cables," IEEE Trans. Dielectr. Electr. Insul., vol. 16, no. 1, pp. 147–154, Feb. 2009.

[9] J. H. Shazly, M. A. Mostafa, D. K. Ibrahim, and E. E. A. E. Zahab, "Thermal analysis of high-voltage cables with several types of insulation for different configurations in the presence of harmonics," Transm. Distrib. IET Gener., vol. 11, no. 14, pp. 3439–3448, 2017.

[10] C. H. Chien and R. W. G. Bucknall, "Analysis of Harmonics in Subsea Power Transmission Cables Used in VSC–HVDC Transmission Systems Operating Under Steady-State Conditions," IEEE Trans. Power Deliv., vol. 22, no. 4, pp. 2489–2497, Oct. 2007.

[11] C. M. Cooke, C. Chryssostomidis, and J. Chalfant, "Modular integrated power corridor," in 2017 IEEE Electric Ship Technologies Symposium (ESTS), 2017, pp. 91–95.